Shear-induced stretching of adsorbed polymer chains

Gui-Li He,*[a] René Messina,[a] Hartmut Löwen,[a] Anton Kiriy,[b] Vera Bocharova[b] and Manfred Stamm[b]

Received 3rd April 2009, Accepted 17th June 2009
First published as an Advance Article on the web 29th June 2009
DOI: 10.1039/b906744b

Shear-induced stretching of polymer chains adsorbed on a planar substrate is explored by atomic force microscopy experiments to visualize chain configurations of a dried spinning droplet containing poly[methacryloyloxyethyl-dimethyl-(3-pyrrol-1-yl-propyl)ammonium bromide] (PME-D-AB) in solution. For increasing shear rates, a considerable proportion of stretched chain configurations is found, which is characterized by an increasing (positive) skewness of the chain size distribution function. This behavior is also reproduced by Brownian dynamics computer simulations if the shear gradient direction is perpendicular to the wall, but not for the situation where the shear vorticity is normal to the wall.

The interaction of large molecules with a substrate is of fundamental interest in many areas of polymer science, engineering and biology. For instance the biocompatibility of implants with blood is determined by this interaction which happens under the shear field of the blood stream.[1] It is also well known that proteins can change their biofunctionality during adsorption to surfaces.[2] Furthermore, for the production of clean water by flocculation of pollution particles, the adsorption of polyelectrolytes and their interactions have to be understood.[3] There are many more examples, but astonishingly enough the interactions and conformational changes of macromolecules during the adsorption process are still not well understood, in particular if this adsorption process occurs under external fields including shear.[4] This may be attributed to the fact that investigations on single molecules and their individual conformations have become only feasible over recent years because of technological advances in microscopy techniques.

From the experimental side many investigations of adsorbed molecules actually focus on investigations of chain conformations in solution. Chains will adapt to the changing boundary conditions and surface interactions.[5–7] As a consequence 2-dimensional conformations differ from the projection of 3-dimensional conformations, and will in addition change with the application of external fields. An understanding of resulting surface conformations thus requires knowing the details of the adsorption process.

Although there are many approaches to describe the adsorption process of polymer molecules and proteins to solid surfaces (see *e.g.* references in ref. 4), there is much less work on the influence of shear during adsorption[8] or adhesion.[9] For weak adsorption, it has been shown that hydrophobic chains[10] and polyelectrolyte molecules[11] are stretched by shear. Recently some papers address the conformational behavior which includes the stretching of end-grafted DNA in a shear field[12] and the structure of polymers under steady shear.[13] Simulations and theory addressed the conformations of sheared chains in the bulk[14–18] and of grafted chains under shear,[19] but adsorbed chains under shear are less studied.[20] Since the process of shearing and drying in the experiment is complex, the two different shear gradient directions are simulated in the models below to understand its effect on the conformational behavior.

In this work, we investigate the conformations of strongly adsorbed chains under shear. A combined study involving an experimental spin coating process and Brownian dynamics computer simulations is proposed. For increasing shear rates, an increasing fraction of the polymers are stretched. The distribution of the polymer extensions is very asymmetric with an increasing positive "skewness" implying that there is a growing long tail with extremely stretched configurations. This is in agreement with our Brownian dynamics computer simulations if the shear gradient is directed perpendicular to the wall. However, the polymer conformational properties change qualitatively if the shear gradient is in-plane (or equivalently the shear vorticity is normal to the wall). In the latter case, stretching is significantly increased compared to the case of the normal shear gradient direction, and the skewness of the distribution function of the polymer size becomes negative.

In the presently conducted experiment, poly[methacryloyloxyethyl-dimethyl-(3-pyrrol-1-yl-propyl) ammonium bromide] (PME-D-AB) ($M_n = 328000$ g/mol; $M_w/M_n = 1.27$) is used as a model polycation at a room temperature of 23 °C. Octylamine is placed directly in the solution of PME-D-AB for hydrophobization of mica: octylamine has a polar amino-group and apolar octyl chain and serves as a surfactant here. It adsorbs faster than larger polymer molecules and weakens attraction of polyelectrolyte chains to mica, making their stretching possible. A solution of PME-D-AB in water and of octylamine in tetrahydrofurane both at concentration of 1 g/l are combined at 1/1 volume ratio and intensively shaken just before the experiment. After that a 20 μl droplet of the prepared solution is placed in the center of a sheet of freshly cleaved mica with the size of 10×8 mm^2 rotating at 33 Hz for 60 s. The sample is then investigated by means of AFM in the dry state at rest. Images are recorded at two different locations, see Fig. 1(a)(b): nearby the rotation center (with distance from the rotation center of $r_I = 720$ μm - region I) and on the periphery of the mica sheet (region II roughly at $r_{II} = 3600$ μm from the rotation center). As can be seen from the corresponding AFM images, the macromolecules close to the center, appear in a much more coiled conformation (Fig. 1(d)), than those located on the periphery (Fig. 1(e)). This feature is consistent with the fact that the "effective" shear rate is five times higher at region II than at I (since $r_{II}/r_I = 3600/720 = 5$). It is important to emphasize that the stretched polymers in region II are aligned along the velocity direction of the rotating plate. This is consistent with the assumption that the main contribution to the shear rate comes from

[a]*Institut für Theoretische Physik II, Heinrich-Heine-Universität Düsseldorf, Universitätsstrasse 1, D-40225 Düsseldorf, Germany. E-mail: guili@thphy.uni-duesseldorf.de*
[b]*Leibniz-Institut für Polymerforschung Dresden, Hohe Strasse 6, D-01069 Dresden, Germany*

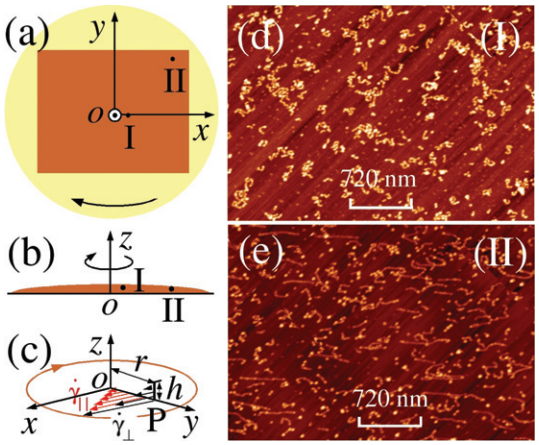

Fig. 1 (a) Schematic diagram of experimentally rotating equipment (top view); (b) Side view of the experimental setup; (c) The sketch of possibly experienced shear by the polymers at the randomly selected location P in the experiment; (d), (e) AFM images of PME-D-AB at the two locations: I (~720 μm from the rotation center *O*) and II (~3600 μm far away from the center).

the retarded motion of the droplet surface relative to the spinning ground which produces high shear rates with a gradient normal to the wall. The ratio of the normal gradient to normal vorticity (*i.e.* centrifugal) shear contribution scales with r/h where h is the thickness of the rotating droplet in z direction and r its distance from the rotation center (Fig. 1(c)). Typically, in the end stage of the drying process, h is getting small such that $r/h >> 1$ implying that shear with normal gradient direction is realized in the experiments.

In order to understand the underlying physics of the polymer conformations, we have carried out non-equilibrium Brownian dynamics computer simulations as well. The model polymer chain is made up of a series of 48 coarse-grained bead-spring monomers. The strong confinement stemming from the drying process in the experiment, is taken into account *via* two parallel walls, of which the bottom wall at $z = 0$ is strongly attractive. The equation of motion for the position $\mathbf{r}_i(t) = (x_i(t), y_i(t), z_i(t))$ of monomer i reads:

$$\mathbf{r}_i(t+\delta t) = \mathbf{r}_i(t) + \frac{D_0}{k_B T}\mathbf{F}_i\delta t + \delta\mathbf{G}_i + \dot{\gamma} q_i(t)\delta t \mathbf{e}_x \qquad (1)$$

with the shear flow being in the x-direction ($\mathbf{e}_x$ denoting the corresponding unit vector) and $\dot{\gamma}$ standing for the shear rate. We have considered two possible and distinct directions for the shear gradient: (i) z-direction [$q_i(t) = z_i(t)$ in eqn (1)] referred to as the normal gradient (NG), see Fig. 4(a); (ii) y-direction [$q_i(t) = y_i(t)$ in eqn (1)] corresponding to a vorticity perpendicular to the wall, denoted NV as sketched in Fig. 4(b). The Gaussian stochastic displacement $\delta\mathbf{G}_i$ assumes a zero mean and a variance $2D_0\delta t$ for each Cartesian component, with D_0 standing for the free diffusion constant. The conservative force $\mathbf{F}_i$ has three contributions: (i) steric effects (monomer–monomer and wall–monomer repulsive interactions) are taken into account *via* a truncated and shifted purely repulsive Lennard-Jones potential $U_{LJ} = 4\varepsilon[(\sigma/r)^{12} - (\sigma/r)^6 - (\sigma/r_c)^{12} + (\sigma/r_c)^6]$ with a cutoff at its minimum $r_c = 2^{1/6}\sigma$. Here, $\varepsilon = k_B T$ (with k_B being the Boltzmann's constant and T the absolute temperature) and σ set the energy and length units, respectively. (ii) The "spring" is modeled *via* a finite extensible nonlinear elastic (FENE)[21] potential $U_{FENE} = -0.5KR_0^2\ln[1 - (r/R_0)^2]$ which ensures the connectivity between adjacent beads along the backbone. We have set the FENE cut-off to $R_0 = 1.5\sigma$ and the spring constant to $K = 27\varepsilon/\sigma^2$. (iii) The adsorption at the bottom wall is mimicked by using a Van der Waals-like strongly attractive potential $U_{ads}(z) = -A_0\varepsilon(\sigma/z)^6$ with $A_0 = 5$. Here surface corrugation is neglected which is a good approximation for the cleaved mica surfaces in the experiment. The BD time step is $\delta t = 2 \times 10^{-6}\tau$, where $\tau = \sigma^2/D_0$. Typically 5×10^8 BD time steps, during which the first 5×10^7 steps are for the chain relaxation, are used for data production.

Simulation snapshots are shown in Fig. 2(a)(b) for a normal shear gradient. At low reduced shear rate ($\dot{\gamma}\tau = 10$), the chain adopts mainly coil conformations. Upon increasing the shear rate ($\dot{\gamma}\tau = 50$), the chain gets considerably elongated. Various types of chain conformations appear including completely stretched ones (Fig. 2(b)(c) line 1), hairpins (line 2–5), V- (line 6–7) and Z- (line 8) shaped configurations and stretched-coiled combinations (line 9–12). It is remarkable that all these individual types are found both in the simulation (see Fig. 2(b)) and experiment (see Fig. 2(c)).

In order to achieve a more quantitative comparison between experiment and simulations, we have analyzed the polymer size distributions. Fig. 3 shows the size distribution for the PME-D-AB molecules located in region I and II. It is observed, for both sample regions I and II, that no bimodal character sets in and that there is a preponderance of coil-sized chains of about 100 nm, compare with Fig. 1(d)(e). However, the distribution is much broader for region II.

As far as BD simulations are concerned, we have considered an analog conformational property.[22] Again, the size distribution $P(L/\sigma)$ (Fig. 4) shows that higher shear rates tend to broaden the size distribution considerably. In the NG case (*i.e.*, transversal shear gradient direction), the size distribution, see Fig. 4(a), exhibits a clear

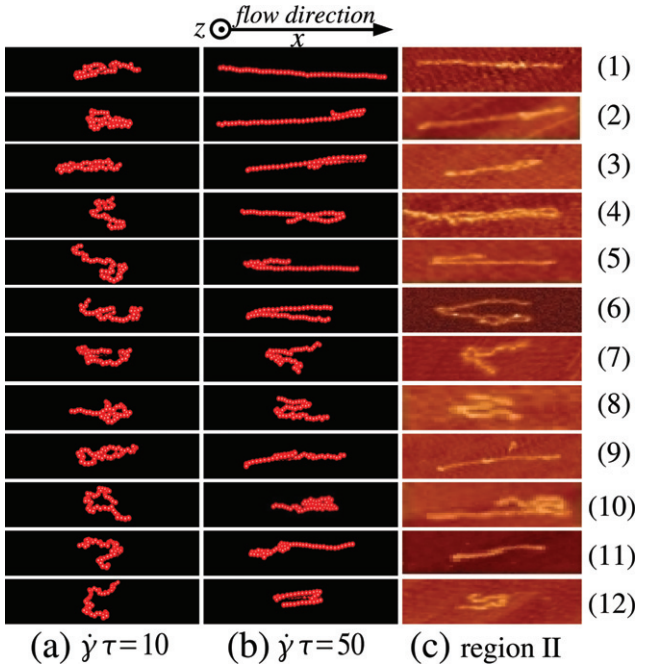

Fig. 2 (a)(b) Typical simulation snapshots of polymer chains under linear shear flow in x-direction. The surface normal is parallel to the shear gradient direction (NG). Here the left column (a) shows configurations for a shear rate $\dot{\gamma}\tau = 10$ (corresponding to Fig. 1(d)), the center column (b) for $\dot{\gamma}\tau = 50$ (corresponding to Fig. 1(e)) and the pictures in the right column (c) are the experimental chain images at location II.

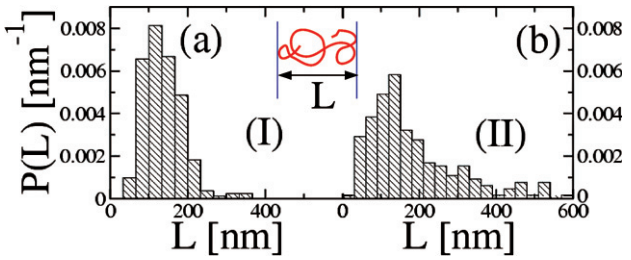

Fig. 3 Distribution $P(L)$ of the maximal chain length L (see inset) of the experimental samples: (a) for the polymers at location I and (b) at II.

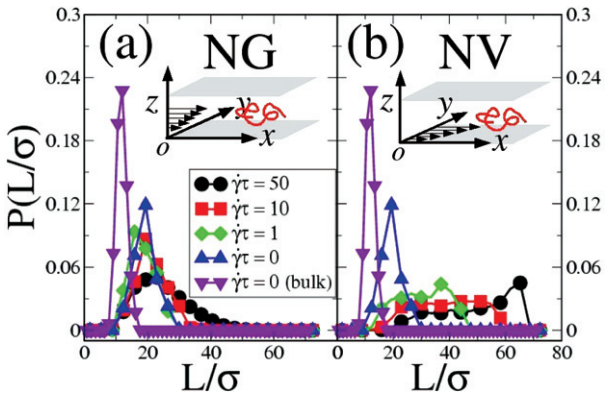

Fig. 4 The distributions of the maximal chain length L under different shear gradient: (a) normal gradient (NG) and (b) normal vorticity (NV).

and unique peak for all investigated values of $\dot{\gamma}\tau$, in good qualitative agreement with the experimental findings of Fig. 3. This demonstrates also the preponderance and stability of coil-sized conformations for the NG model. The situation becomes qualitatively different if one considers an in-plane shear gradient direction (*i.e.*, the NV case) as depicted in Fig. 4(b). More precisely, upon increasing $\dot{\gamma}\tau$, the maximum in $P(L/\sigma)$ gets shifted to larger chain size. At the highest shear rate $\dot{\gamma}\tau = 50$, the size distribution indicates a strong proportion of fully stretched conformations (Fig. 4(b)), in contrast to the NG case (Fig. 4(a)).

In probability theory and statistics,[23] the so-called *skewness* parameter S measures the asymmetry of the probability distribution function. It is defined as $S = \mu_3/\sigma^3_s$,[23] where μ_3 is the third moment with respect to the mean and σ_s is the standard deviation. For a sample of n values $\{s_i\}$, the skewness is given by

$$S = \frac{\frac{1}{n}\sum_{i=1}^{n}(s_i - \bar{s})^3}{\left\{\frac{1}{n}\sum_{i=1}^{n}(s_i - \bar{s})^2\right\}^{3/2}} \qquad (2)$$

where $\bar{s}$ designates the sample mean. The skewnesses of the chain size distributions from Fig. 4 are reported in Fig. 5(a). If the shear gradient is normal to the wall (NG model), the skewness S is positive and increases with shear rate. This positivity of S is a quantitative signature of the statistical preponderance of the coiled conformations in the NG model. Conversely, for shear vorticity normal to the wall (NV model), the skewness S is negative and decreases with shear rate revealing the preponderance of fully stretched configurations.

The physical origin of the sign difference in S (Fig. 5(a)) for different shear gradient directions (NG or NV) is due to the strong

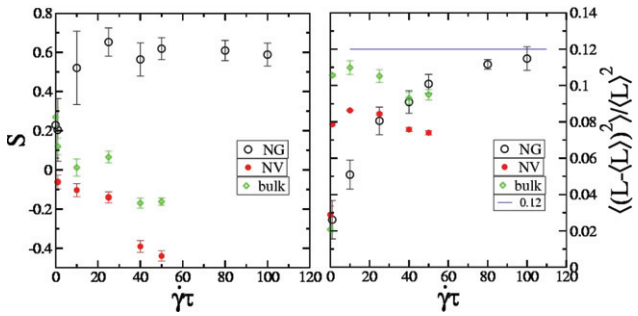

Fig. 5 (a) Skewness S of the maximal chain length distribution $P(L/\sigma)$ for the NG (○), NV (●) and bulk case (◇); (b) The rescaled second moment with respect to the mean. The error bars were calculated over five independent simulation runs.

adsorption of the polymer chain. Indeed, there are only weak fluctuations of the monomers in the z-direction, as it is also experimentally the case. Therefore the chain is much more responsive to the two-dimensional in-plane flow (*i.e.*, the NV case) than to the normal one (*i.e.*, the NG case). In this limit, the NV case can be seen as an almost perfect two-dimensional stretching. The experimental values for S in region I and II are $S_I = 1.08$ and $S_{II} = 1.24$, which are positive and in good agreement with the values found in the simulations for the NG model. This is consistent with our previous argument that the dominant component of the shear gradient is normal to the substrate.

We have included the skewness of the chain size distribution in the three-dimensional bulk under linear shear flow as well, see the diamonds in Fig. 5(a) which are different from the confined cases. This gives clear evidence that the statistics of an adsorbed chain is different from that obtained by projecting simple bulk conformations.

To better quantify the experimental data and the results of the simulations, the rescaled second moment is also plotted in Fig. 5(b). Here the solid line stands for the corresponding value for the chains located at region I in the experiments, which approximately match the simulation data at $\dot{\gamma}\tau \approx 100$. The chain relaxation time is 65τ in the simulation and roughly 0.01 s in the experiment. From this we estimate a shear rate in the experiment of 6×10^5 s^{-1} consistent with what is expected in a sub-micrometre thin spinning droplet at a frequency of 33 s^{-1}.

In conclusion, we analyzed conformations of strongly adsorbed polymer chains using both atomic force microscopy experiments and Brownian dynamics computer simulations. We find considerably stretched polymer chains along the shear flow with a wealth of different individual shapes. The asymmetry of the polymer size distribution characterized by the skewness is in good agreement between simulation and experiment under the assumption that the shear gradient is normal to the wall. The main conclusion is that the polymer configurations found in the experiments are vastly different from projected three-dimensional bulk configurations but consistent with strongly adsorbed ones under the steady-state condition of an imposed linear shear gradient normal to the wall. This implies that only the late-stage process of drying leads to a simple projection of adsorbed configurations. This is relevant for applications ranging from the imaging of proteins and protein complexes[24] to the coffee ring problem.[25] Finally our simulations revealed that shear flow with vorticity normal to the wall leads to configurations which are fully stretched. This suggests the use of microfluidic devices[26] in order to

generate strongly stretched polymer chains which are helpful for the construction of microcircuits from single polymer molecules.[27]

Acknowledgements

We thank K. Huber and R. Winkler for helpful discussions. This work was supported by the DFG *via* LO 418/12 and STA 324/23.

Notes and references

1 B. D. Ratner and S. J. Bryant, *Ann. Rev. Biomed. Eng.*, 2004, **6**, 41.
2 F. Rusmini, Z. Y. Zhong and J. Feijen, *Biomacromolecules*, 2007, **8**, 1775.
3 M. B. Hocking, K. A. Klimchuk and S. Lowen, *Polym. Rev.*, 1999, **39**(2), 177.
4 N. Hoda and S. Kumar, *J. Chem. Phys.*, 2008, **128**, 164907.
5 C. Rivetti, M. Guthold and C. Bustamante, *J. Mol. Biol.*, 1996, **264**, 919.
6 S. Minko, A. Kiriy, G. Gorodyska and M. Stamm, *J. Am. Chem. Soc.*, 2002, **124**, 3218.
7 L. J. Kirwan, G. Papastavrou, M. Borkovec and S. H. Behrens, *Nano Lett.*, 2004, **4**, 149.
8 S. C. Bae and S. Granick, *Ann. Rev. Phys. Chem.*, 2007, **56**, 353.
9 S. W. Schneider, S. Nuschele, A. Wixforth, C. Gorzelanny, A. Alexander-Katz, R. R. Netz and M. F. Schneider, *Proc. Natl. Acad. Sci. U. S. A.*, 2007, **104**, 7899.
10 J. J. L. M. Cornelissen, J. J. J. M. Donners, G. Metselaar, R. de Gelder, W. S. Graswinckel, A. E. Rowan, N. A. J. M. Sommerdijk and R. J. M. Nolte, *Science*, 2001, **293**, 676.
11 V. Bocharova, A. Kiriy, M. Stamm, F. Stoffelbach, R. Jrme and C. Detrembleur, *Small*, 2006, **2**, 910.
12 A. Bensimon, A. Simon, A. Chiffaudel, V. Croquette, F. Heslot and D. Bensimon, *Science*, 1994, **265**, 2096.
13 P. P. Jose and G. Szamel, *J. Chem. Phys.*, 2007, **127**, 114905.
14 B. Ladoux and P. S. Doyle, *Europhys. Lett.*, 2000, **52**, 511.
15 S. Gerashchenko and V. Steinberg, *Phys. Rev. Lett.*, 2006, **96**, 038304.
16 R. Delgado-Buscalioni, *Phys. Rev. Lett.*, 2006, **96**, 088303.
17 C. M. Schroeder, R. E. Teixeira, E. S. G. Shaqfeh and S. Chu, *Phys. Rev. Lett.*, 2005, **95**, 018301.
18 A. Celani, A. Puliafito and K. Turitsyn, *Europhys. Lett.*, 2005, **70**(4), 464.
19 A. Alexander-Katz, M. F. Schneider, S. W. Schneider, A. Wixforth and R. R. Netz, *Phys. Rev. Lett.*, 2006, **97**, 138101.
20 N. Hoda and S. Kumar, *J. Chem. Phys.*, 2007, **127**, 234902.
21 K. Kremer and G. S. Grest, *J. Chem. Phys.*, 1990, **92**, 5057.
22 Note: By simulations, we confirmed the distribution of the end-to-end distance $P(R_e)$ is highly similar to P(L).
23 D. N. Joanes and C. A. Gill, *J. R. Stat. Soc. Ser. D: Stat.*, 1998, **47**(1), 183.
24 L. S. Shlyakhtenko, A. A. Gall, A. Filonov, Z. Cerovac, A. Lushnikov and Y. L. Lyubchenko, *Ultramicroscopy*, 2003, **97**(1–4), 279.
25 R. D. Deegan, O. Bakajin, T. F. Dupont, G. Huber, S. R. Nagel and T. A. Witten, *Nature*, 1997, **389**(6653), 827.
26 S. Koster, D. Steinhauser and T. Pfohl, *J. Phys.: Condens. Matter*, 2005, **17**(49), S4091.
27 A. Knobloch, A. Manuelli, A. Bernds and W. Clemens, *J. Appl. Phys.*, 2004, **96**, 2286.